Heteronuclear double resonance in nuclear magnetic resonance spectroscopy: Relaxation of multiple-quantum coherences

Simone Ulzega,[1] Mariachiara Verde,[1] Fabien Ferrage,[2,a)] and Geoffrey Bodenhausen[1,2]
[1]*Ecole Polytechnique Fédérale de Lausanne, Institut des Sciences et Ingénierie Chimiques, Lausanne 1015, Switzerland*
[2]*Département de Chimie, Ecole Normale Supérieure, associé au CNRS, 24 rue Lhomond, 75231 Paris Cedex 05, France*

(Received 19 August 2009; accepted 7 November 2009; published online 9 December 2009)

Theoretical and experimental investigations of the relaxation rates of multiple-quantum coherences during heteronuclear double resonance (HDR) pulse sequences are presented. Average Liouvillian theory yields analytical expressions to describe the effective relaxation rates of multiple-quantum coherences during HDR irradiation. Experiments were carried out on a $^{13}C-^{1}H$ pair in glycerol to measure the effective auto- and cross-relaxation rates of multiple-quantum coherences during HDR schemes. The experimental results exhibit a very good agreement with theoretical predictions, even when the average Liouvillian expansion is truncated to zeroth order.
 [doi:10.1063/1.3269044]

I. INTRODUCTION

NMR is one of the most versatile tools to sample and quantify the internal dynamics of molecules and, in particular, of biomolecules.[1,2] NMR has proven to be suitable for the characterization of processes such as conformational exchange and chemical reactions that occur on microsecond to millisecond timescales which lead to so-called chemical exchange effects.[3,4] The study of NMR relaxation caused by chemical exchange has led to the determination of the kinetics and thermodynamics of many exchange processes as well as the structural characterization[5–7] of the conformations that are involved in exchange. An ever-growing range of methods is available to measure chemical-exchange-induced relaxation of nitrogen-15 single-quantum (SQ) coherences.[8,9] Correlated chemical exchange processes can be detected thanks to their signature on the relaxation of multiple-quantum (MQ) coherences.[10,11] A breakthrough early in this decade was achieved through the introduction of methods to quantify such effects.[12–14] Techniques derived from this approach have opened the way to the interpretation of exchange processes beyond the basic two-state model[15] and provided evidence for the correlation of conformational exchange between sequential residues.[16,17]

The two most common approaches to characterize chemical-exchange-induced relaxation rates are measurements of transverse relaxation rates under Carr–Purcell–Meiboom–Gill trains of spin echoes[18–20] and measurements of rotating-frame relaxation rates under a continuous wave (cw) irradiation.[9,21–23] The former method is perfectly adapted to the study of slow (millisecond) time-scale processes and has been used to quantify both SQ and MQ relaxation.[24–26] While rotating-frame "spin-locking" methods give access to a much broader range of time scales,[27] they were hitherto not suitable to study MQ relaxation.

We have recently introduced new HDR methods to preserve MQ coherences.[28] We have shown that spin locking or, more accurately, "preservation" of MQ coherences can be made effective over a range of offsets comparable to the radio frequency (rf) amplitude for most scalar-coupling constants found in biomolecules, with little sensitivity to rf field inhomogeneities. Here, we present a detailed description of relaxation during HDR sequences in the absence of chemical exchange. In Sec. II we briefly introduce average Liouvillian theory (ALT)[29,30] and apply it to treat the effective relaxation of MQ coherences under HDR sequences. In Sec. III, experimental evidence of the validity of this theoretical approach is demonstrated for isolated $^{13}C-^{1}H$ pairs found in 98% perdeuterated glycerol. These results are then briefly discussed in Sec. IV.

II. THEORY

A. Introduction

The effective auto- and cross-relaxation rates in pairs of spin-1/2 nuclei under homonuclear double-resonance irradiation has been treated in the case of synchronous nutation,[31,32] albeit without providing a simple analytical expression of the effective relaxation superoperator. In the case of heteronuclear cross polarization, a full Liouvillian superoperator was derived to describe both coherent effects and relaxation during mismatch-optimized transfer[33,34] and during single-transition cross polarization,[35,36] in both cases in liquids. In these two studies, a zeroth-order perturbation theory was used, neglecting nonsecular terms in the relevant interaction frames. This approach is robust when the coherent terms are much larger than the relaxation rates, as in our HDR schemes where the rf field amplitudes are generally larger than 1 kHz. Here, we present a zeroth-order ALT approach to the study of effective relaxation rates of MQ coherences during HDR sequences. As shown below, this method leads to compact analytical expressions for the average relaxation superoperators.

a)Electronic mail: fabien.ferrage@ens.fr.

TABLE I. Experimental values of relaxation rates of the isolated $^{13}C^2-{}^1H^2$ pair in D8-glycerol (98%) in ^2H_2O. All values are given in s^{-1}. Experiments were carried out on two different samples and at different temperatures, as described in the text. Four different data sets were recorded, as shown in the leftmost column. The first three data sets were obtained with a TCI cryoprobe, while the fourth set was recorded with the TBI probe. The relaxation rates ρ_{IS}, ρ_S^a, ρ_I^a, and λ_{MQ} were measured with the methods shown in Fig. 1. The values of the effective MQ autorelaxation rates λ_{xx}^{MLEV} and λ_{yy}^{MLEV} predicted by ALT (second column from the right) were derived from these four relaxation rates using Eqs. (13a) and (13b). These two effective autorelaxation rates under MLEV-32 HDR were measured (rightmost column) with the sequence shown in Fig. 1(f). The comparison between ALT predictions and experimental MLEV-32 HDR rates, shown in the last two columns on the right, is also rendered graphically in Fig. 3.

	ρ_{IS}	ρ_S^a	ρ_I^a	λ_{MQ}	i ($2H_iC_i$)	λ_{ii}^{MLEV} ALT	λ_{ii}^{MLEV} HDR
1. T=281.5 K sample 1	2.58(2)	3.50(5)	3.15(12)	2.61(11)	x	2.69(8)	2.68(8)
					y	2.78(5)	2.73(15)
2. T=284.0 K sample 2	2.66(2)	4.10(3)	4.21(11)	2.55(4)	x	2.77(3)	2.84(4)
					y	2.99(3)	3.02(11)
3. T=281.0 K sample 2	2.69(2)	4.93(3)	4.85(11)	2.72(2)	x	2.99(2)	3.03(3)
					y	3.25(2)	3.28(4)
4. T=273.0 K sample 1	2.58(2)	5.10(3)	5.26(3)	2.98(9)	x	3.18(2)	3.15(8)
					y	3.38(3)	3.46(9)

B. The average Liouvillian approach

Let us consider a scalar-coupled heteronuclear two-spin system, with $I=1/2$ (usually an isolated proton) and $S=1/2$ (often a ^{13}C or ^{15}N nucleus). The evolution of the density operator $\sigma(t)$ is governed by a quantum mechanical master equation,[37] i.e., a Liouville–von Neumann equation including relaxation, which may be written in terms of superoperators in the convenient homogeneous form[38]

$$\frac{d}{dt}\sigma(t) = -\hat{L}\sigma(t) \tag{1}$$

with the Liouvillian superoperator $\hat{L}$ defined as

$$\hat{L} = i\hat{H} + \hat{\Gamma}. \tag{2}$$

In the above equation $\hat{H}$ is the commutator superoperator defined as $\hat{H}\sigma=[H,\sigma]$, where H is the doubly rotating frame (DRF) Hamiltonian[28] of the system, and $\hat{\Gamma}$ is the relaxation superoperator which includes the thermal correction for finite temperature.[29,30,39] In this paper carets will denote superoperators. The density operator $\sigma(t)$ can be expanded in an orthonormal basis of operators B_i, with coefficients $\sigma_i(t)$,

$$\sigma(t) = \sum_{i=1}^{D} \sigma_i(t)B_i. \tag{3}$$

For a system of two spin-1/2 nuclei, the dimension of the Liouville operator space, or simply Liouville "superspace," is $D=16$. The density operator is thus represented in the Liouville superspace as a column vector with 16 elements corresponding to the 16 coefficients σ_i. We found it to be convenient for our applications to choose a basis set of Cartesian product operators, including the unity operator (see Appendix). The elements of the matrix representation of the coherent part $i\hat{H}$ of the master Eq. (1) are given by[39]

$$i\hat{H}^{(s,r)} = \langle B_s|i\hat{H}|B_r\rangle = \langle B_s|[iH,B_r]\rangle = iTr[B_s^\dagger(HB_r - B_rH)] \tag{4}$$

with $s,r=1,\ldots,16$, while the matrix elements of the relaxation superoperator can be calculated in the framework of Redfield theory,[40] as clearly described by Cavanagh *et al.*[41] Explicit matrix forms of $i\hat{H}$ and $\hat{\Gamma}$ can be found in the Appendix.

In order to evaluate the perturbations to the dominant interaction, the Liouvillian superoperator $\hat{L}$ is transformed into the interaction frame of the corresponding Hamiltonian $i\hat{H}$. This frame transformation can be accomplished in analogy to Hamiltonians.[41] One may thus define a transformed density operator in the new interaction frame (denoted by the subscript if) as

$$\sigma_{if}(t) = \hat{U}_0(t)\sigma(t), \quad \text{with} \quad \hat{U}_0(t) = \exp[i\hat{H}t]. \tag{5}$$

The master Eq. (1) can then be rewritten in the interaction frame as

$$\frac{d}{dt}\sigma_{if}(t) = -\hat{L}_{if}(t)\sigma_{if}(t), \quad \text{where} \quad \hat{L}_{if}(t) = \hat{U}_0(t)\hat{L}\hat{U}_0^\dagger(t) - i\hat{H}. \tag{6}$$

It is straightforward to verify that $\hat{L}_{if}(t)=\hat{U}_0(t)\hat{\Gamma}\hat{U}_0^\dagger(t)$. If $i\hat{H}$ is periodic with a period T, the effect of the relaxation superoperator $\hat{\Gamma}$ in the interaction frame can be described by average Liouvillian theory,[29,30] provided the system is sampled stroboscopically. The formalism is very similar to the one of average Hamiltonian theory[42,43] that we have outlined in a preceding publication on the same subject.[28] The average

Liouvillian may be defined using the Magnus expansion as

$$\hat{L}_{\mathrm{if}}^{(\mathrm{av})} = \hat{L}_{\mathrm{if}}^{(0)} + \hat{L}_{\mathrm{if}}^{(1)} + \hat{L}_{\mathrm{if}}^{(2)} + \ldots, \tag{7}$$

where the zeroth-order term is defined as

$$\hat{L}_{\mathrm{if}}^{(0)} = \frac{1}{T}\int_0^T \hat{L}_{\mathrm{if}}(t)dt. \tag{8}$$

In this paper we shall treat only the lowest order term of the average Liouvillian.

C. Average Liouvillian during HDR pulse sequences

Recently, we have presented[28] two new HDR sequences based on the well-known MLEV-32 and WALTZ-32 decoupling schemes,[44–48] and we have shown that, in the absence of relaxation, these HDR sequences render MQ coherences such as $2I_xS_x$ and $2I_yS_y$ effectively stationary over a reasonably wide range of offsets and scalar-coupling constants. In the present work, relaxation is taken into account but scalar couplings are neglected, and both rf fields are applied on resonance. We may start with the expression of the Liouvillian superoperator $\hat{L}$ of Eq. (2) in the DRF

$$\hat{L} = i\hat{H}_{\mathrm{rf}} + \hat{\Gamma}, \tag{9}$$

where the rf Liouvillian superoperator $i\hat{H}_{\mathrm{rf}}$ is obtained by replacing H by $H_{\mathrm{rf}}[\phi_I(t), \phi_S(t)]$ (Ref. 28) in Eq. (4). The explicit matrix representation of $i\hat{H}_{\mathrm{rf}}$ can be found in the Appendix. We shall assume that the superoperator $\hat{L}$ is time independent. This condition is fulfilled during each pulse of the sequence provided the phases ϕ_I and ϕ_S are constant. The effect of relaxation during the pulse sequence can be studied by rewriting the relaxation superoperator in the interaction frame of the rf fields.[34] The calculations are the same as for Hamiltonian operators, described in detail elsewhere.[28] One can show that the zeroth-order average Liouvillian $\hat{\Gamma}_{\mathrm{if}}^{(0)}$ of Eq. (8) can be calculated over a period $T=64\pi/\omega_1$ or $T=96\pi/\omega_1$, as the sum of 96 or 72 integrals corresponding to the number of pulses of the MLEV-32 or WALTZ-32 HDR sequences, respectively. The forms of both MLEV-32 and WALTZ-32 HDR sequences lead to a coincidence of the rf interaction frame and the DRF at the end of each period T. The average effect of relaxation over an integer number of periods T may then be obtained by the integration of

$$\frac{d}{dt}\sigma(t) = -\hat{\Gamma}_{\mathrm{if}}^{(0)}\sigma(t). \tag{10}$$

D. The zeroth-order effect

In the absence of rf fields, the dynamics of MQ coherences under the relaxation superoperator $\hat{\Gamma}$ are described by the following differential equations:

$$\frac{d}{dt}\begin{bmatrix} 2I_xS_x \\ 2I_yS_y \end{bmatrix} = -\begin{bmatrix} \lambda_{\mathrm{MQ}} & -\mu_{\mathrm{MQ}} \\ -\mu_{\mathrm{MQ}} & \lambda_{\mathrm{MQ}} \end{bmatrix}\begin{bmatrix} 2I_xS_x \\ 2I_yS_y \end{bmatrix}, \tag{11}$$

where λ_{MQ} and μ_{MQ} are the auto- and cross-relaxation rates, respectively. The average Liouvillian of Eq. (10) yields for the dynamics of MQ coherences during either MLEV-32 or WALTZ-32 HDR sequences

$$\frac{d}{dt}\begin{bmatrix} 2I_xS_x \\ 2I_yS_y \end{bmatrix} = -\begin{bmatrix} \lambda_{xx}^{K} & -\mu_{\mathrm{MQ}}^{K} \\ -\mu_{\mathrm{MQ}}^{K} & \lambda_{yy}^{K} \end{bmatrix}\begin{bmatrix} 2I_xS_x \\ 2I_yS_y \end{bmatrix}, \tag{12}$$

with K=MLEV or WALTZ, and

$$\lambda_{xx}^{\mathrm{MLEV}} = \frac{1}{16}(11\lambda_{\mathrm{MQ}} + \rho_I^a + \rho_S^a + 3\rho_{IS}), \tag{13a}$$

$$\lambda_{yy}^{\mathrm{MLEV}} = \frac{1}{16}(6\lambda_{\mathrm{MQ}} + 2\rho_I^a + 2\rho_S^a + 6\rho_{IS}), \tag{13b}$$

$$\mu_{\mathrm{MQ}}^{\mathrm{MLEV}} = \frac{1}{16}(\lambda_{\mathrm{MQ}} + 4\mu_{\mathrm{MQ}} - \rho_I^a - \rho_S^a + \rho_{IS}), \tag{13c}$$

$$\lambda_{xx}^{\mathrm{WALTZ}} = \lambda_{\mathrm{MQ}}, \tag{14a}$$

$$\lambda_{yy}^{\mathrm{WALTZ}} = \frac{1}{8}(3\lambda_{\mathrm{MQ}} + \rho_I^a + \rho_S^a + 3\rho_{IS}), \tag{14b}$$

$$\mu_{\mathrm{MQ}}^{\mathrm{WALTZ}} = \mu_{\mathrm{MQ}}/2, \tag{14c}$$

where $\rho_I^a(\rho_S^a)$ is the transverse autorelaxation rate for spin I (S) coherence in antiphase with respect to spin S (I), $2I_xS_z(2I_zS_x)$, and ρ_{IS} is the autorelaxation rate of the longitudinal two-spin order $2I_zS_z$.[39] These equations show that the HDR pulse sequences induce *effective* MQ auto- and cross-relaxation rates. Note that the effective relaxation matrices associated with both MLEV-32 and WALTZ-32 HDR schemes are symmetric, i.e., the effective rates are the same for the two directions of the cross-relaxation pathway between the MQ coherences $2I_xS_x$ and $2I_yS_y$.

The effective relaxation rates are linear combinations of several auto- and cross-relaxation rates of SQ and MQ coherences as well as of the decay rate of two-spin order, and can be associated with density operator terms evolving during the pulse sequences in a seven-dimensional subspace of the Liouville superspace, i.e., in a subspace spanned by the operators $2I_zS_x$, $2I_xS_z$, $2I_zS_y$, $2I_yS_z$, $2I_xS_x$, $2I_yS_y$, and $2I_zS_z$. Note that the MLEV-32 HDR sequence attenuates the true cross-relaxation rate μ_{MQ} by a factor of 4, while the WALTZ-32 HDR sequence only scales down μ_{MQ} by a factor of 2. Moreover, one may also observe that $\mu_{\mathrm{MQ}}^{\mathrm{WALTZ}}$ is directly proportional to the "natural" cross-relaxation rate μ_{MQ}, whereas $\mu_{\mathrm{MQ}}^{\mathrm{MLEV}}$ is "contaminated" by a combination of several other relaxation rates. The exploitation of effective cross-relaxation rates measured under HDR sequences is therefore more straightforward with the WALTZ-32 HDR rather than MLEV-32 HDR sequence. One should notice that

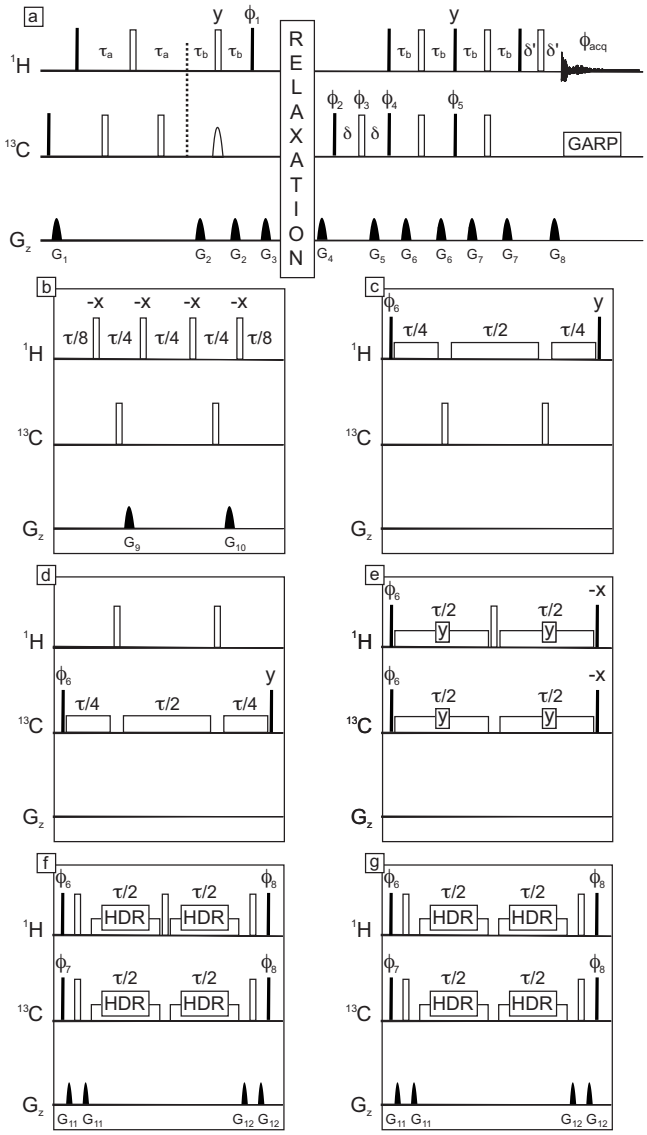

FIG. 1. Pulse sequences used for the measurement of relaxation rates. (a) Generic pulse sequence for the preparation and the detection of various two-spin coherences or longitudinal two-spin order $2H_zC_z$. [(b)–(g)] Pulse sequences used during the relaxation delay τ for the measurement of relaxation rates: (b) ρ_{IS} of the two-spin order $2H_zC_z$; (c) ρ_I^a of the SQ antiphase proton coherence $2H_xC_z$; (d) ρ_S^a of the SQ antiphase carbon-13 coherence $2H_zC_x$; (e) λ_{MQ} of the MQ coherence $2H_yC_y$; and for the measurement of (f) the effective autorelaxation rates $\lambda_{xx}^{\mathrm{MLEV}}$ and $\lambda_{yy}^{\mathrm{MLEV}}$, defined in Eq. (13); and (g) the effective cross-relaxation $\mu_{\mathrm{MQ}}^{\mathrm{WALTZ}}$ or $\mu_{\mathrm{MQ}}^{\mathrm{MLEV}}$ between the MQ coherence $2H_xC_x$ and $2H_yC_y$. Narrow (filled) and wide (open) rectangles represent 90° and 180° pulses, respectively. Pulse phases are along the x axis of the rotating frame unless specified otherwise. The bell-shaped pulse represents a 1.2 ms Gaussian inversion pulse. The delays are τ_a=50 ms, τ_b=1.786 ms, δ=1.4 ms, and δ'=1.3 ms. Strong pulses were applied with a rf amplitude of 14.2 kHz on the proton channel and 15.1 kHz on the carbon-13 channel. Spin lock and HDR irradiations were applied with an amplitude of 1.5 kHz on both channels. Decoupling during acquisition with a duration of 130 ms was carried out with a GARP (Ref. 58) scheme and a 2.27 kHz rf amplitude. The delay between experiments was 1.5 s. The carrier was set at 3.49 ppm on the ^{1}H channel and 71.61 ppm on the ^{13}C channel. For each spectrum, 384 transients were accumulated. The pulsed field gradients had sine-bell-shaped amplitude profiles. Their durations and peak amplitudes over the x, y, and z axes were, respectively: G_1; 500 μs, 0, 0, 11 G cm^{-1}; G_2; 500 μs, 8 G cm^{-1}, 0, 0; G_3; 500 μs, 40 G cm^{-1}, 40 G cm^{-1}, 25 G cm^{-1}; G_4; 1.5 ms, 0, 0, −15 G cm^{-1}; G_5; 1 ms, 0 G cm^{-1}, 0 G cm^{-1}, 40 G cm^{-1}; G_6; 500 μs, 0 G cm^{-1}, 6 G cm^{-1}, 0 G cm^{-1}; G_7; 500 μs, 5 G cm^{-1}, 0 G cm^{-1}, 0 G cm^{-1}; G_8; 1 ms, 0 G cm^{-1}, 0 G cm^{-1}, 10 G cm^{-1}; G_9; 500 μs, 25 G cm^{-1}, 20 G cm^{-1}, 0 G cm^{-1}; G_{10}; 500 μs, 20 G cm^{-1}, 0 G cm^{-1}, 28 G cm^{-1}; G_{11}; 300 μs, 9 G cm^{-1}, 0 G cm^{-1}, 9 G cm^{-1}; G_{12}; 300 μs, 0 G cm^{-1}, 8 G cm^{-1}, 8 G cm^{-1}. Gradient pulses employed on the TCI cryoprobe had the same shapes, durations, and comparable amplitudes but were all applied along the z axis. The phase cycles were: (b) $\phi_1=\{y,-y\}$; [(c)–(g)] $\phi_1=\{y\}$; [(b)–[(d)] $\phi_2=\{x\}$; [(e)–(g)] $\phi_2=4\{x\},4\{-x\}$; [(b)–(d)] $\phi_3=2\{x\},2\{y\},2\{-x\},2\{-y\}$; [(e)–(g)] $\phi_3=\{x\}$; (b) $\phi_4=8\{x\},8\{-x\}$; [(c) and (d)] $\phi_4=\{x\}$; [(e)–(g)] $\phi_4=8\{x\},8\{-x\}$; (b) $\phi_5=8\{-y\},8\{y\}$; [(c) and (d)] $\phi_5=-y$; [(e)–(g)] $\phi_5=8\{y\},8\{-y\}$; [(c) and (d)] $\phi_6=\{y,-y\}$; (e) $\phi_6=\{x,-x\}$. To generate the MQ coherence $2H_xC_x$ at the beginning of the relaxation period, the phases in experiments (f) and (g) were $\phi_6=\{y,-y\}$ and $\phi_7=2\{y\},2\{-y\}$. To generate the MQ coherence $2H_yC_y$ the phases in experiments (f) and (g) were $\phi_6=\{x,-x\}$ and $\phi_7=2\{x\},2\{-x\}$. To detect the MQ coherence $2H_xC_x$ at the end of the relaxation period, the phase in experiments (f) and (g) was $\phi_8=\{y\}$. To detect the MQ coherence $2H_yC_y$ at the end of the relaxation period, the phase in experiments (f) and (g) was $\phi_8=\{x\}$. Finally, the phase cycles for acquisition were (b) $\phi_{\mathrm{acq}}=2\{x,-x,-x,x\},2\{-x,x,x,-x\}$; [(c) and (d)] $\phi_{\mathrm{acq}}=2\{x,-x,-x,x\}$; (e) $\phi_{\mathrm{acq}}=4\{x\},8\{-x\},4\{x\}$; [(f) and (g)] $\phi_{\mathrm{acq}}=\{x,-x,-x,x\},2\{-x,x,x,-x\},\{x,-x,-x,x\}$.

the effective autorelaxation rates for the two MQ coherences of interest are different: $\lambda_{xx}^{\mathrm{MLEV}} \neq \lambda_{yy}^{\mathrm{MLEV}}$ and $\lambda_{xx}^{\mathrm{WALTZ}} \neq \lambda_{yy}^{\mathrm{WALTZ}}$. This feature is of particular importance in cross-relaxation experiments, as it makes the use of symmetrical reconversion[49,50] necessary to average the auto-relaxation rates of the two observed MQ coherences.

III. EXPERIMENTS

A. MQ autorelaxation rates

All experiments were carried out on the residual (about 0.02%) isolated $^{13}C^2-^1H^2$ pair in 98% perdeuterated D8-glycerol ($CD_2OD^{13}CHODCD_2OD$) mixed with ^2H_2O. Two different samples, 1 and 2, were prepared with (w/w) ratios of glycerol and ^2H_2O of 75/25 and 80/20, respectively. The viscosities of samples 1 and 2 are about 35 and 65 cP, respectively, at $T=293$ K. All data were collected in a static magnetic field $B_0=14.1$ T with a Bruker Avance 600 MHz spectrometer, equipped either with a triple resonance inverse probehead (TBI) or with a triple resonance cryoprobe (TCI). The use of the cryoprobe improves the sensitivity of the experiments but imposes serious limitations on the stability of the sample temperature below 281 K. Therefore, we have used the cryoprobe in three series of experiments at $T=284$ K (with sample 2), $T=281.5$ K (sample 1), and $T=281$ K (sample 2). Below 281 K, we observed oscillations of the temperature on the order of ± 1 K. An additional series of experiments at $T=273$ K (with sample 1) was run with the more stable TBI probe. The four series of experiments are summarized in Table I.

A series of independent experiments were carried out to measure the auto-relaxation rates λ_{MQ}, ρ_S^a, ρ_I^a, and ρ_{IS}. All these rates were measured with pulse sequences derived from our original HDR sequence[28] by replacing the HDR block with the sequences shown in Fig. 1. The signal of the central $^{13}C^2-^1H^2$ pair in glycerol was selected while suppressing the signals of the two $^{13}C^1-^1H^1$ isotopomers. The latter show a faster transverse relaxation due to a large contribution of scalar relaxation of the second kind.[22,51] Indeed, the one-bond $^1J(^{13}C^1-^2H^1)$ scalar coupling is significantly larger than the two-bond $^2J(^{13}C^2-^2H^1)$ scalar coupling. Selection was carried out by two complementary mechanisms. First, to make use of the faster autorelaxation of the $^1H_y^1$ coherence compared to the $^1H_y^2$ coherence, a 100 ms echo was inserted at the beginning of the sequence. Second, a selective 1.2 ms Gaussian inversion pulse was applied to the carbon channel in the first sequence based on 'Insensitive Nuclei Enhanced by Polarization Transfer' (INEPT). To measure the autorelaxation rate constant ρ_{IS} of the two-spin order term $2H_zC_z$ we replaced the original HDR block with the scheme[52] of Fig. 1(b). In our sample, coherences have a rapid autorelaxation rate because of the scalar relaxation of the second kind induced by the one bond or two-bond scalar coupling with ^2H nuclei. In order to suppress this contribution all relaxation rates of coherences were measured under a continuous irradiation with rf fields with an amplitude $\omega_1/(2\pi)$ of 1.5 kHz. We have measured the relaxation rates $\rho_S^a(\rho_I^a)$ of the antiphase coherences $2H_zC_x(2H_xC_z)$ with a cw spin-lock field applied to $^{13}C(^1H)$, and the autorelaxation rate λ_{MQ} of the MQ coherence $2H_xC_x$ with two cw spin-lock fields applied to both nuclei simultaneously [see Figs. 1(c)–1(e)]. Experiments designed for the measurement of anti-phase coherences [Figs. 1(c) and 1(d)] feature a pair of inversion pulses to suppress cross-relaxation pathways due to the cross-correlation of chemical shift anisotropy (CSA) and dipole-dipole (DD) interactions.[53,54] Similarly, a single inversion pulse was applied in Fig. 1(e) to suppress the effects of the weak cross-relaxation between the operators $2H_yC_y$ and $2H_xC_x$. A far off-resonance irradiation was added at the beginning of all sequences featuring a continuous irradiation during the relaxation delay [Figs. 1(c)–1(g)] to ensure comparable heating by rf fields for all durations of the relaxation delays.[55,56]

In order to verify the validity of ALT predictions, we have also carried out direct measurements of the two autorelaxation rates λ_{xx}^{MLEV} and λ_{yy}^{MLEV} (rightmost column of Table I). These rates were measured with the modified HDR pulse sequence shown in Fig. 1(f), by selecting either $2H_xC_x$ or $2H_yC_y$ before the relaxation block. The HDR sequence, which consists of a windowless sequence of rf pulses applied simultaneously on both nuclei ^{13}C and ^1H, allows one to preserve the coherences of interest and suppress scalar-relaxation effects. The original HDR sequence was modified [see Fig. 1(f)], in addition to the temperature compensation scheme, by inserting a single π pulse in the middle of the relaxation delays to remove cross-relaxation effects so that the decays of the coherences of interest can be fitted by monoexponential functions.[53,54]

B. MQ cross-relaxation rates

As discussed at the end of Sec. II D, measurements of effective cross-relaxation rates with the MLEV-32 HDR sequence are rather impractical compared to the WALTZ-32 HDR method. We have thus applied the latter scheme to measure the effective cross-relaxation rate μ_{MQ}^{WALTZ}. This rate is simply proportional to the "true" cross-relaxation rate in the absence of any rf irradiation, μ_{MQ}, as shown in Eq. (14c). The experiments were run with sample 2, with an rf field strength $\omega_1/(2\pi)$ of 1.5 kHz, at a temperature $T=281$ K, using the cryoprobe. The pulse sequence is shown in Fig. 1(g). As discussed in Sec. II D, we used symmetrical reconversion[49,50] in order to compensate for the different effective autorelaxation rates λ_{xx}^{WALTZ} and λ_{yy}^{WALTZ}. By selecting either $2H_xC_x$ or $2H_yC_y$ before and after the relaxation delay, one obtains four different measurements for each relaxation delay τ. Thus we first selected $2H_xC_x$ at the beginning and measured $2H_xC_x$ (signal s_1) and $2H_yC_y$ (signal s_2) after the delay τ, then we selected $2H_yC_y$ at the beginning and measured $2H_xC_x$ (signal s_3) and $2H_yC_y$ (signal s_4) after relaxation. The signal $S(\tau)$ (Fig. 4) is given by

$$S(\tau)=\sqrt{\frac{s_2s_3}{s_1s_4}}. \tag{15}$$

This observable can be fitted with the function

$$f(\tau)=\tanh\left|\mu_{MQ}^{WALTZ}\tau\right|=\tanh\left|\frac{\mu_{MQ}}{2}\tau\right|, \tag{16}$$

represented by a dashed line in Fig. 4. In the above equation we have exploited the fact that $\mu_{MQ}^{WALTZ}=\mu_{MQ}/2$.

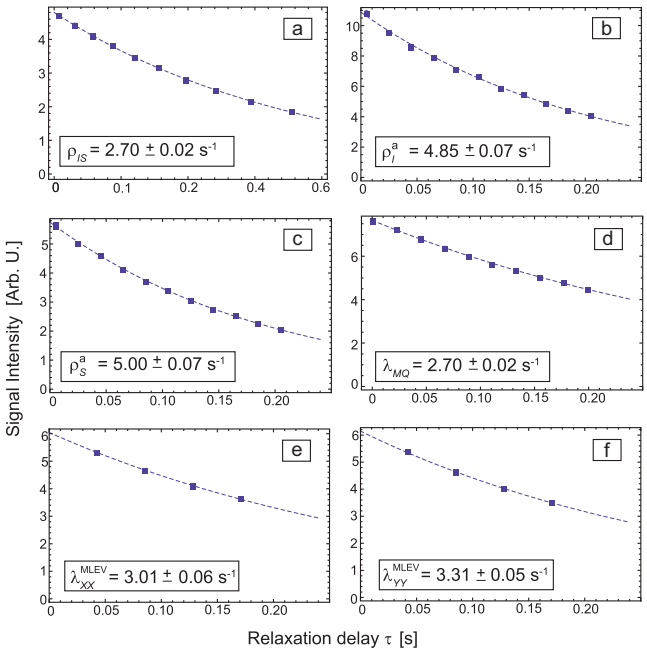

FIG. 2. Examples of experimental decays of various two-spin terms: (a) $2H_zC_z$, with rate ρ_{IS}, (b) $2H_xC_z$, with rate ρ_I^a, (c) $2H_zC_x$, with rate ρ_S^a, (d) $2H_xC_x$, with rate λ_{MQ}, measured with the pulse sequences [(b)–(e)] of Fig. 1. (e) Effective autorelaxation of the MQ coherence $2H_xC_x$, with rate λ_{xx}^{MLEV}, and (f) decay of $2H_yC_y$, with rate λ_{yy}^{MLEV}, measured with the HDR pulse sequences (f) and (g) of Fig. 1. All relaxation rates (in boxes) were obtained by fitting the experimental decays with monoexponential functions, shown as dashed lines. All data refer to experiments on sample 2 (relative w/w concentration of glycerol and ^2H_2O of 80/20) at $T=281$ K. The error bars are smaller than the symbol size.

IV. RESULTS AND DISCUSSION

A. Autorelaxation rates

Examples of experimental decays due to autorelaxation of two-spin order, antiphase, and MQ coherences are shown in Figs. 2(a)–2(d). If we insert the experimental autorelaxation rates in Eqs. (13a) and (13b) we obtain the values of λ_{xx}^{MLEV} and λ_{yy}^{MLEV} predicted by zeroth-order ALT (see Table I). Here we shall consider mostly the MLEV-32 HDR scheme rather than the WALTZ-32 HDR because the former is less sensitive to scalar-coupling constants[28] $^1J_{CH}$. This makes the use of WALTZ-32 HDR potentially less accurate in the $^{13}C-^1H$ pairs of glycerol with scalar-coupling constants $^1J_{CH}\approx 140$ Hz.

The experimental decays of $2H_xC_x$ and $2H_yC_y$ are shown in Figs. 2(e) and 2(f), while the resulting values of λ_{xx}^{MLEV} and λ_{yy}^{MLEV} are shown in Table I. The two rightmost columns of Table I allow us to compare the experimental effective relaxation rates observed during the MLEV-32 HDR sequence with the predictions of the zeroth-order ALT of Sec. II D. A graphical representation of these results is given in Fig. 3. We found a good global agreement between experiments and theory.

It is interesting to note that the demonstration of the agreement of experiments with ALT depends on the difference of the effective autorelaxation rates associated with the MQ operators $2H_xC_x$ and $2H_yC_y$. This difference depends on the various auto-relaxation rates that appear in the expressions of λ_{xx}^{MLEV} and λ_{yy}^{MLEV} [see Eqs. (13a) and (13b)]. We

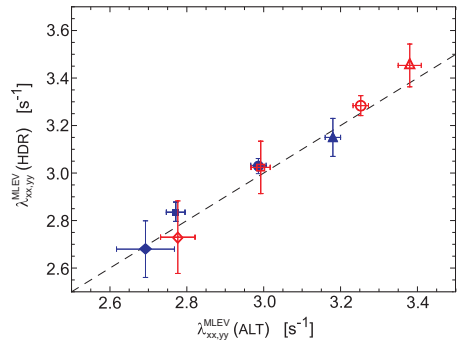

FIG. 3. Comparison between zeroth-order ALT predictions (horizontally) and experimental results obtained with MLEV-32 HDR pulse sequences (vertically). The data shown here correspond to the last two columns of Table I. Filled (blue) and open (red) symbols correspond to MQ coherences $2H_xC_x$ and $2H_yC_y$, respectively. Referring to Table I, diamonds correspond to data set (1), squares to set (2), circles to set (3), and triangles to set (4). Details about these different data sets are given in Table I and in the text. The dashed line represents the ideal agreement of ALT predictions and experimental HDR data.

observed that the separate determination of the two relaxation rates, and thus the quality of our results, can be improved significantly by increasing the viscosity of the sample, i.e., either by reducing its temperature or by increasing the concentration of glycerol. At $T=293$ K, the viscosity of sample 1 is about 35 cP, while it is 65 cP for sample 2. A similar increase in viscosity can be achieved by reducing the temperature of either sample by about 10 K. For example, at $T=283$ K, the viscosity of sample 1 is about 65 cP, while for sample 2 it is about 120 cP. These effects are visible in Fig. 3.

The agreement between the effective relaxation rates measured with the MLEV-32 HDR sequence and the effective rates predicted by ALT is excellent, both for λ_{xx}^{MLEV} and λ_{yy}^{MLEV} under all conditions. These results strongly support the zeroth-order ALT approach as well as the conclusions of our earlier study of the coherent evolution of MQ coherences under the MLEV-32 HDR sequence.[28] Indeed, the suppression of coherent evolution is a prerequisite for measuring clean autorelaxation rates. Here, the effective rates measured with MLEV-32 HDR are not systematically larger than those predicted by ALT based on independent relaxation measurements. This shows that the pulse sequence preserves all MQ coherences very well and cancels the effects of scalar couplings or rf inhomogeneities even for durations as long as 100 ms.

B. Cross-relaxation rates

Figure 4 shows the buildup of the observable of Eq. (15) resulting from symmetrical reconversion using the WALTZ-32 HDR scheme of Fig. 1(g). The fit of the experimental data points [see Eq. (16)] gives $\mu_{MQ}=0.76\pm 0.07$ s^{-1}.

This estimate of the true cross-relaxation rate can be incorporated into the expression of the effective cross-relaxation rate under the MLEV-32 HDR sequence, μ_{MQ}^{MLEV} of Eq. (13c). From the measured auto-relaxation rates in Table I, one can estimate

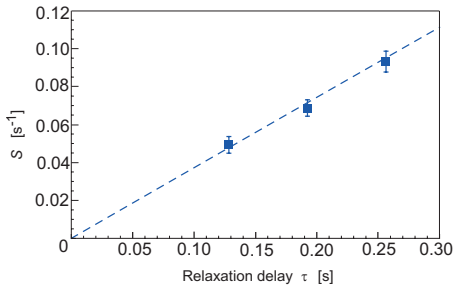

FIG. 4. Measurement of the effective cross-relaxation rate μ_{MQ}^{WALTZ} that governs the interconversion of the operators $2H_xC_x$ and $2H_yC_y$. The definition of the symmetrical reconversion observable S is given in Eq. (15). The dashed line represents the fitting function of Eq. (16).

$$\mu_{MQ}^{MLEV}(ALT) = 0.072 \pm 0.025 \ \ s^{-1}. \tag{17}$$

It is remarkable that the auto- and cross-relaxation rates that appear in the expression of μ_{MQ}^{MLEV} tend to cancel each other, leading to a very small effective cross-relaxation rate. Indeed, measurements of the effective cross-relaxation rate under the MLEV-32 HDR method turned out to be difficult. As expected, the nearly vanishing effective cross-relaxation rate caused the intensity of the cross-relaxed signal to emerge barely above the noise. The resulting poor signal-to-noise ratio (between 1.5 and 2) caused an obvious deterioration of the quality of the build-up curve, compared to the equivalent WALTZ-32 HDR experiment (see Fig. 4). We have carried out several measurements of μ_{MQ}^{MLEV} with symmetrical reconversion, following the scheme outlined in Sec. III B, by selecting either $2H_xC_x$ or $2H_yC_y$ at the beginning and at the end of the fixed relaxation delay $T=128$ ms. The average value of the effective relaxation rate was

$$\mu_{MQ}^{MLEV}(HDR) = 0.034 \pm 0.020 \ \ s^{-1}. \tag{18}$$

This is in good agreement with the estimate given in Eq. (17). If one excludes the accidental compensation of systematic errors in both HDR measurements, this result validates both the ALT prediction of cross-relaxation rates and the measurement of effective cross-relaxation rates using either of the two HDR sequences.

The accuracy of the measurement of cross-relaxation rates under symmetrical reconversion is very robust. For instance, even if the cross-relaxing operators are allowed to undergo a small effective coherent evolution, the experimental rates are hardly affected, provided the coherent evolution does not lead to an interconversion between the two operators. Similarly, it does not require the quenching of all other cross-relaxation pathways, provided that there is no other pathway for the interconversion between cross-relaxing operators.[50] As seen in our previous study[28] and the preceding section, relaxation studies using the MLEV-32 HDR sequence do not suffer from any of these potential drawbacks. On the other hand, the preservation of MQ coherences under the WALTZ-32 HDR sequence is not expected to be perfect when the scalar-coupling constant is significantly larger than 100 Hz. Nevertheless, our experimental observations show that cross relaxation between the operators $2H_xC_x$ and $2H_yC_y$ can be measured accurately with symmetrical reconversion.

V. CONCLUSIONS

We have demonstrated that relaxation of MQ coherences under HDR sequences could be predicted accurately by average Liouvillian theory. A number of effective auto- and cross-relaxation rates have been determined separately in the subsystem comprising the two operators $2H_xC_x$ and $2H_yC_y$. The simple relationship between the effective cross-relaxation rate during the WALTZ-32 HDR sequence μ_{MQ}^{WALTZ} and the true cross-relaxation rate in the absence of any irradiation μ_{MQ} makes the analysis of WALTZ-32 HDR data straightforward. The effect of coherent interactions and relaxation processes on MQ coherences during HDR sequences is well understood. Systems undergoing chemical exchange, where the contribution of exchange to the effective relaxation rates depends on the amplitude of the rf fields, will be investigated in a complementary study.

ACKNOWLEDGMENTS

This work was supported by the Swiss National Science Foundation (FNRS), the Swiss Commission for Technology and Innovation (CTI), the French CNRS, and the Programme blanc (Grant No. NT05-4_43730) of the French Agence Nationale de la Recherche (ANR).

APPENDIX: LIOUVILLE SUPEROPERATORS

In Liouville operator space, or simply Liouville superspace, the density operator $\sigma(t)$ describing a system of N spin-1/2 nuclei is expanded in an orthonormal basis of operators B_i, with coefficients $\sigma_i(t)$, as shown in Eq. (3), where $D=4^N$ is the dimension of the Liouville superspace. Here we consider the case of a heteronuclear scalar-coupled two-spin system, $I=1/2$ and $S=1/2$, for which $D=16$. Consequently, the Liouville representation of the density operator is a column vector of 16 elements, which correspond to the coefficients σ_i of Eq. (3). We have chosen a basis set $B=\{B_i\}_{i=1,\ldots,16}$ of Cartesian product operators,[57] including the unity operator $\mathcal{E}$

$$B = \{\mathcal{E}/2, I_x, I_y, I_z, S_x, S_y, S_z, 2I_xS_z, 2I_yS_z, 2I_zS_x, 2I_zS_y, 2I_xS_x, 2I_xS_y, 2I_yS_x, 2I_yS_y, 2I_zS_z\}. \tag{A1}$$

Moreover, the usual Dirac bracket product has to be redefined in the larger Liouville superspace as

$$\langle B_r | B_s \rangle = Tr[B_r^\dagger B_s]. \tag{A2}$$

An element (s,r) of the matrix representation of the Hamiltonian superoperator $i\hat{H}$ of the master equation [Eq. (1)] of the two-spin system is given by[37,39] Eq. (4). In the Cartesian basis [Eq. (A1)] of the DRF, $i\hat{H}$ can be written as

$$\begin{bmatrix}
0 & 0 & 0 & 0 & 0 & 0 & 0 & 0 & 0 & 0 & 0 & 0 & 0 & 0 & 0 & 0 \\
0 & 0 & \Omega_I & -\omega_1 \mathbb{S}_I & 0 & 0 & 0 & 0 & \pi J_{IS} & 0 & 0 & 0 & 0 & 0 & 0 & 0 \\
0 & -\Omega_I & 0 & \omega_1 \mathbb{C}_I & 0 & 0 & 0 & -\pi J_{IS} & 0 & 0 & 0 & 0 & 0 & 0 & 0 & 0 \\
0 & \omega_1 \mathbb{S}_I & -\omega_1 \mathbb{C}_I & 0 & 0 & 0 & 0 & 0 & 0 & 0 & 0 & 0 & 0 & 0 & 0 & 0 \\
0 & 0 & 0 & 0 & 0 & \Omega_S & -\omega_1 \mathbb{S}_S & 0 & 0 & 0 & \pi J_{IS} & 0 & 0 & 0 & 0 & 0 \\
0 & 0 & 0 & 0 & -\Omega_S & 0 & \omega_1 \mathbb{C}_S & 0 & 0 & -\pi J_{IS} & 0 & 0 & 0 & 0 & 0 & 0 \\
0 & 0 & 0 & 0 & \omega_1 \mathbb{S}_S & -\omega_1 \mathbb{C}_S & 0 & 0 & 0 & 0 & 0 & 0 & 0 & 0 & 0 & 0 \\
0 & 0 & \pi J_{IS} & 0 & 0 & 0 & 0 & 0 & \Omega_I & 0 & 0 & \omega_1 \mathbb{S}_S & -\omega_1 \mathbb{C}_S & 0 & 0 & -\omega_1 \mathbb{S}_I \\
0 & -\pi J_{IS} & 0 & 0 & 0 & 0 & 0 & -\Omega_I & 0 & 0 & 0 & 0 & 0 & \omega_1 \mathbb{S}_S & -\omega_1 \mathbb{C}_S & \omega_1 \mathbb{C}_I \\
0 & 0 & 0 & 0 & 0 & \pi J_{IS} & 0 & 0 & 0 & 0 & \Omega_S & \omega_1 \mathbb{S}_I & 0 & -\omega_1 \mathbb{C}_I & 0 & -\omega_1 \mathbb{S}_S \\
0 & 0 & 0 & 0 & -\pi J_{IS} & 0 & 0 & 0 & 0 & -\Omega_S & 0 & 0 & \omega_1 \mathbb{S}_I & 0 & -\omega_1 \mathbb{C}_I & \omega_1 \mathbb{C}_S \\
0 & 0 & 0 & 0 & 0 & 0 & 0 & -\omega_1 \mathbb{S}_S & 0 & -\omega_1 \mathbb{S}_I & 0 & 0 & \Omega_S & \Omega_I & 0 & 0 \\
0 & 0 & 0 & 0 & 0 & 0 & 0 & \omega_1 \mathbb{C}_S & 0 & 0 & -\omega_1 \mathbb{S}_I & -\Omega_S & 0 & 0 & \Omega_I & 0 \\
0 & 0 & 0 & 0 & 0 & 0 & 0 & 0 & -\omega_1 \mathbb{S}_S & \omega_1 \mathbb{C}_I & 0 & -\Omega_I & 0 & 0 & \Omega_S & 0 \\
0 & 0 & 0 & 0 & 0 & 0 & 0 & 0 & \omega_1 \mathbb{C}_S & 0 & \omega_1 \mathbb{C}_I & 0 & -\Omega_I & -\Omega_S & 0 & 0 \\
0 & 0 & 0 & 0 & 0 & 0 & 0 & \omega_1 \mathbb{S}_I & -\omega_1 \mathbb{C}_I & \omega_1 \mathbb{S}_S & -\omega_1 \mathbb{C}_S & 0 & 0 & 0 & 0 & 0
\end{bmatrix} \tag{A3}$$

with $\mathbb{S}_k = \sin[\phi_k(t)]$ and $\mathbb{C}_k = \cos[\phi_k(t)]$, where ϕ_k $(k=I,S)$ is the phase of the rf fields (as defined in our preceding publication[28]), ω_1 is the angular nutation frequency of the rf fields, $\Omega_k = \omega_k - \omega_{\mathrm{rf}}^k (k=I,S)$ is the angular frequency offset, ω_k and $\omega_{\mathrm{rf}}^k (k=I,S)$ are the Larmor and carrier angular frequencies, respectively, and J_{IS} is the scalar coupling constant. We have assumed that the angular nutation frequency ω_1 is the same for spin I and S.

The explicit matrix representation of the Liouville rf superoperator $i\hat{H}_{\mathrm{rf}}$ can be obtained by applying Eq. (4), with H replaced by the rf Hamiltonian operator[28] $H_{\mathrm{rf}}[\phi_I(t), \phi_S(t)]$. Practically, one can simply retain in Eq. (A3) only the terms that are proportional to the rf nutation angular frequency ω_1 and set all the others equal to zero.

The matrix elements of the relaxation superoperator $\hat{\Gamma}$ can be calculated in the framework of Redfield theory,[40] as clearly described by Cavanagh *et al.*[41] We have carried out explicit calculations assuming that the spin system experiences relaxation due to the direct dipole-dipole coupling of spins I and S (DD autocorrelation contribution) and to the chemical shift anisotropy of either spin I or S (CSA autocorrelation contributions). Moreover, we have taken into account the contributions due to cross correlation between DD and CSA interactions, and the contribution to the autorelaxation of spin I of DD couplings of spin I (typically a proton) with neighboring spins other than S (typically other protons). Following the notation of Allard *et al.*,[39] the calculations yield for $\hat{\Gamma}$

$$\hat{\Gamma} = \begin{bmatrix}
0 & 0 & 0 & 0 & 0 & 0 & 0 & 0 & 0 & 0 & 0 & 0 & 0 & 0 & 0 & 0 \\
0 & \rho_I^{in} & 0 & 0 & 0 & 0 & 0 & \eta_I & 0 & 0 & 0 & 0 & 0 & 0 & 0 & 0 \\
0 & 0 & \rho_I^{in} & 0 & 0 & 0 & 0 & 0 & \eta_I & 0 & 0 & 0 & 0 & 0 & 0 & 0 \\
-2\Theta_I & 0 & 0 & \rho_I & 0 & 0 & \sigma & 0 & 0 & 0 & 0 & 0 & 0 & 0 & 0 & \delta_I \\
0 & 0 & 0 & 0 & \rho_S^{in} & 0 & 0 & 0 & 0 & \eta_S & 0 & 0 & 0 & 0 & 0 & 0 \\
0 & 0 & 0 & 0 & 0 & \rho_S^{in} & 0 & 0 & 0 & 0 & \eta_S & 0 & 0 & 0 & 0 & 0 \\
-2\Theta_S & 0 & 0 & \sigma & 0 & 0 & \rho_S & 0 & 0 & 0 & 0 & 0 & 0 & 0 & 0 & \delta_S \\
0 & \eta_I & 0 & 0 & 0 & 0 & 0 & \rho_I^a & 0 & 0 & 0 & 0 & 0 & 0 & 0 & 0 \\
0 & 0 & \eta_I & 0 & 0 & 0 & 0 & 0 & \rho_I^a & 0 & 0 & 0 & 0 & 0 & 0 & 0 \\
0 & 0 & 0 & 0 & \eta_S & 0 & 0 & 0 & 0 & \rho_S^a & 0 & 0 & 0 & 0 & 0 & 0 \\
0 & 0 & 0 & 0 & 0 & \eta_S & 0 & 0 & 0 & 0 & \rho_S^a & 0 & 0 & 0 & 0 & 0 \\
0 & 0 & 0 & 0 & 0 & 0 & 0 & 0 & 0 & 0 & 0 & \lambda_{\mathrm{MQ}} & 0 & 0 & -\mu_{\mathrm{MQ}} & 0 \\
0 & 0 & 0 & 0 & 0 & 0 & 0 & 0 & 0 & 0 & 0 & 0 & \lambda_{\mathrm{MQ}} & \mu_{\mathrm{MQ}} & 0 & 0 \\
0 & 0 & 0 & 0 & 0 & 0 & 0 & 0 & 0 & 0 & 0 & 0 & \mu_{\mathrm{MQ}} & \lambda_{\mathrm{MQ}} & 0 & 0 \\
0 & 0 & 0 & 0 & 0 & 0 & 0 & 0 & 0 & 0 & 0 & -\mu_{\mathrm{MQ}} & 0 & 0 & \lambda_{\mathrm{MQ}} & 0 \\
-2\Theta_{IS} & 0 & 0 & \delta_I & 0 & 0 & \delta_S & 0 & 0 & 0 & 0 & 0 & 0 & 0 & 0 & \rho_{IS}
\end{bmatrix}. \tag{A4}$$

The leftmost column of $\hat{\Gamma}$ has been introduced *ad hoc* and represents the thermal correction,[29] which accounts for the longitudinal polarization at thermal equilibrium and allows one to write the master equation of the system in its homogeneous form. In Eq. (A4), $\rho_{I,S}$ and σ are longitudinal autorelaxation and cross-relaxation rates, respectively; $\rho_{I,S}^{in}$ and $\rho_{I,S}^{a}$ are transverse in-phase and antiphase relaxation rates, respectively; λ_{MQ} and μ_{MQ} are autorelaxation and cross-relaxation rates of MQ coherences, respectively; ρ_{IS} is the relaxation rate of longitudinal two-spin order; $\eta_{I,S}$ and $\delta_{I,S}$ are longitudinal and transverse cross-correlation relaxation rates, respectively, due to the interference between DD and CSA relaxation mechanisms. There is also a CSA/CSA cross-correlation contribution, which appears only in the MQ cross-relaxation rate μ_{MQ}. Explicit analytical expressions for the various relaxation rates can be found elsewhere.[39]

[1] A. G. Palmer, Annu. Rev. Biophys. Biomol. Struct. **30**, 129 (2001).
[2] A. Mittermaier and L. E. Kay, Science **312**, 224 (2006).
[3] A. D. Bain, Prog. Nucl. Magn. Reson. Spectrosc. **43**, 63 (2003).
[4] A. G. Palmer, M. J. Grey, and C. Y. Wang, Methods Enzymol. **394**, 430 (2005).
[5] T. I. Igumenova, U. Brath, M. Akke, and A. G. Palmer, J. Am. Chem. Soc. **129**, 13396 (2007).
[6] P. Vallurupalli, D. F. Hansen, E. Stollar, E. Meirovitch, and L. E. Kay, Proc. Natl. Acad. Sci. U.S.A. **104**, 18473 (2007).
[7] P. Vallurupalli, D. F. Hansen, and L. E. Kay, Proc. Natl. Acad. Sci. U.S.A. **105**, 11766 (2008).
[8] A. G. Palmer, Chem. Rev. **104**, 3623 (2004).
[9] A. G. Palmer and F. Massi, Chem. Rev. **106**, 1700 (2006).
[10] A. Wokaun and R. R. Ernst, Mol. Phys. **36**, 317 (1978).
[11] M. Rance, J. Am. Chem. Soc. **110**, 1973 (1988).
[12] M. Tessari and G. W. Vuister, J. Biomol. NMR **16**, 171 (2000).
[13] K. Kloiber and R. Konrat, J. Biomol. NMR **18**, 33 (2000).
[14] D. Früh, J. R. Tolman, G. Bodenhausen, and C. Zwahlen, J. Am. Chem. Soc. **123**, 4810 (2001).
[15] D. M. Korzhnev, P. Neudecker, A. Mittermaier, V. Y. Orekhov, and L. E. Kay, J. Am. Chem. Soc. **127**, 15602 (2005).
[16] A. Majumdar and R. Ghose, J. Biomol. NMR **28**, 213 (2004).
[17] P. Lundstrom, F. A. A. Mulder, and M. Akke, Proc. Natl. Acad. Sci. U.S.A. **102**, 16984 (2005).
[18] H. Y. Carr and E. M. Purcell, Phys. Rev. **94**, 630 (1954).
[19] S. Meiboom and D. Gill, Rev. Sci. Instrum. **29**, 688 (1958).
[20] Z. Luz and S. Meiboom, J. Chem. Phys. **39**, 366 (1963).
[21] C. Deverell, R. E. Morgan, and J. H. Strange, Mol. Phys. **18**, 553 (1970).
[22] A. Abragam, *Principles of Nuclear Magnetism* (Oxford University Press, Oxford, 1983).
[23] H. Desvaux and P. Berthault, Prog. Nucl. Magn. Reson. Spectrosc. **35**, 295 (1999).
[24] J. Dittmer and G. Bodenhausen, J. Am. Chem. Soc. **126**, 1314 (2004).
[25] V. Y. Orekhov, D. M. Korzhnev, and L. E. Kay, J. Am. Chem. Soc. **126**, 1886 (2004).
[26] J. Wist, D. Frueh, J. R. Tolman, and G. Bodenhausen, J. Biomol. NMR **28**, 263 (2004).
[27] F. Massi, E. Johnson, C. Wang, M. Rance, and A. G. Palmer, J. Am. Chem. Soc. **126**, 2247 (2004).
[28] M. Verde, S. Ulzega, F. Ferrage, and G. Bodenhausen, J. Chem. Phys. **130**, 074506 (2009).
[29] M. H. Levitt and L. Di Bari, Phys. Rev. Lett. **69**, 3124 (1992).
[30] R. Ghose, Concepts Magn. Reson. **12**, 152 (2000).
[31] I. Burghardt, R. Konrat, B. Boulat, S. J. F. Vincent, and G. Bodenhausen, J. Chem. Phys. **98**, 1721 (1993).
[32] B. Boulat, I. Najfeld, and M. Rance, J. Magn. Reson., Ser. A **120**, 223 (1996).
[33] M. H. Levitt, D. Suter, and R. R. Ernst, J. Chem. Phys. **84**, 4243 (1986).
[34] M. H. Levitt, J. Chem. Phys. **94**, 30 (1991).
[35] F. Ferrage, T. R. Eykyn, and G. Bodenhausen, J. Chem. Phys. **113**, 1081 (2000).
[36] T. R. Eykyn, F. Ferrage, and G. Bodenhausen, J. Chem. Phys. **116**, 10041 (2002).
[37] R. R. Ernst, G. Bodenhausen, and A. Wokaun, *Principles of Nuclear Magnetic Resonance in One and Two Dimensions* (Oxford University Press, Oxford, 1987).
[38] R. Jeener, Adv. Magn. Reson. **10**, 1 (1982).
[39] P. Allard, M. Helgstrand, and T. Härd, J. Magn. Reson. **134**, 7 (1998).
[40] A. G. Redfield, Adv. Magn. Reson. **1**, 1 (1965).
[41] J. Cavanagh, W. J. Fairbrother, A. G. Palmer III, M. Rance, and N. J. Skelton, *Protein NMR Spectroscopy*, 2nd ed. (Academic, San Diego, 2007).
[42] W. Magnus, Commun. Pure Appl. Math. **7**, 649 (1954).
[43] U. Haeberlen and J. S. Waugh, Phys. Rev. **175**, 453 (1968).
[44] M. H. Levitt and R. Freeman, J. Magn. Reson. **43**, 502 (1981).
[45] M. H. Levitt, R. Freeman, and T. Frenkiel, J. Magn. Reson. **47**, 328 (1982).
[46] M. H. Levitt, Prog. Nucl. Magn. Reson. Spectrosc. **18**, 61 (1986).
[47] R. Freeman, *Spin Choreography: Basic Steps in High Resolution NMR* (Oxford University Press, Oxford, 1998).
[48] A. J. Shaka, J. Keeler, T. Frenkiel, and R. Freeman, J. Magn. Reson. **52**, 335 (1983).
[49] P. Pelupessy, G. M. Espallargas, and G. Bodenhausen, J. Magn. Reson. **161**, 258 (2003).
[50] P. Pelupessy, F. Ferrage, and G. Bodenhausen, J. Chem. Phys. **126**, 134508 (2007).
[51] S. Grzesiek and A. Bax, J. Am. Chem. Soc. **116**, 10196 (1994).
[52] C. Wang, M. J. Grey, and A. G. Palmer, J. Biomol. NMR **21**, 361 (2001).
[53] A. G. Palmer, N. J. Skelton, W. J. Chazin, P. E. Wright, and M. Rance, Mol. Phys. **75**, 699 (1992).
[54] L. E. Kay, L. K. Nicholson, F. Delaglio, A. Bax, and D. A. Torchia, J. Magn. Reson. **97**, 359 (1992).
[55] A. C. Wang and A. Bax, J. Biomol. NMR **3**, 715 (1993).
[56] G. N. B. Yip and E. R. P. Zuiderweg, J. Magn. Reson. **176**, 171 (2005).
[57] O. W. Sørensen, G. W. Eich, M. H. Levitt, G. Bodenhausen, and R. R. Ernst, Prog. Nucl. Magn. Reson. Spectrosc. **16**, 163 (1984).
[58] A. J. Shaka, P. B. Barker, and R. Freeman, J. Magn. Reson. **64**, 547 (1985).